Optimal Design for Higher Resistance to Thermal Impulse: A Lesson Learned from the Shells of Deep-sea Hydrothermal-vent Snails

Anran Wei,[1] Ding Yuan,[1,3] Bingzhi He,[1] Yujie Xie,[1] Andre E. Vellwock,[1] Jin Sun,[4] and Haimin Yao[1,2,5]

[1] Laboratory for Bio-inspired Mechanics and Structures, Department of Mechanical Engineering, The Hong Kong Polytechnic University, Kowloon, Hong Kong, China

[2] Research Center for Fluid-Structure Interactions, Department of Mechanical Engineering, The Hong Kong Polytechnic University, Kowloon, Hong Kong, China

[3] Department of Mechanical & Electrical Engineering, Xiamen University, Xiamen 361005, China

[4] Institute of Evolution & Marine Biodiversity, Ocean University of China, Qingdao 266003, China

[5] e-mail: mmhyao@polyu.edu.hk

Abstract

Inspired by the unique layered structure and the superior resistance to thermal impulse exhibited by the shells of snails inhabiting the deep-sea hydrothermal environment, here we attempt to reveal the underlying structure-property relationship by investigating the temperature response of a bilayer subjected to a thermal impulse on one side. A semi-analytical solution to the transient temperature field is obtained, allowing us to examine the effects of the layout sequence and volume fractions of the constitutive layers on the thermal impulse resistance of the shell. For two layers made of given materials, the proper layout sequence and optimal thickness ratio are proposed, giving rise to the highest resistance to thermal impulse. The results of our work not only account for the physiological functionality of the unique laminated design of the snail shells from deep-sea hydrothermal environments but also provide operational guidelines for the development of thermal barriers in engineering.

Keywords: Thermal barrier; Thermal conductivity; Laminated composites; Bio-inspiration; Biomimetics

INTRODUCTION

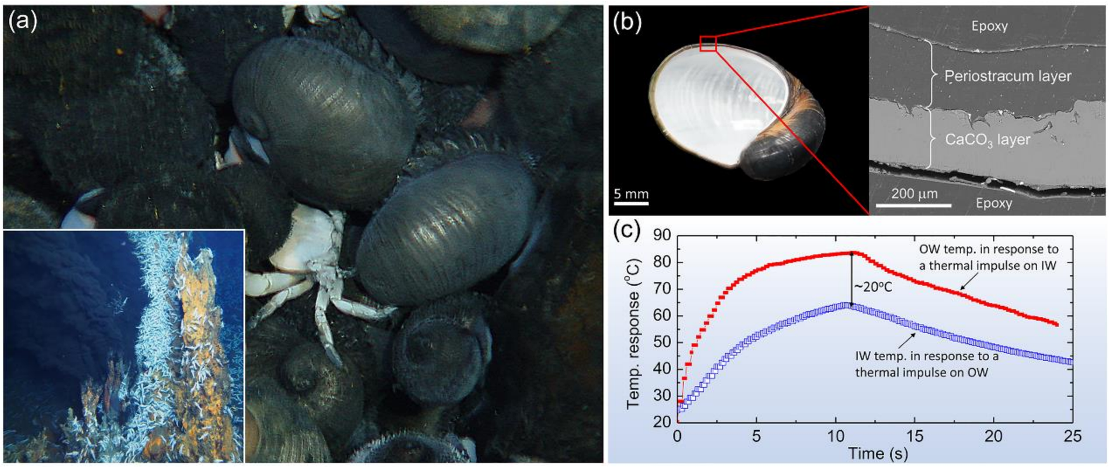

Fig. 1 (**a**) Photos of scaly-foot snails (*Chrysomallon squamiferum*) inhabiting in the vicinity of Kairei hot vent field (inset). Photo courtesy of JAMSTEC. (**b**) A photo and cross-sectional SEM image of the shell of a scaly-foot snail (*C. squamiferum*) collected from Longqi hydrothermal vent field (see Materials and Methodology). (**c**) Measured temperature response on one side of the shell in (**b**) to a thermal impulse of ~88 ℃ applied on the opposite side for a duration of ~11 s. OW: outer wall, IW: inner wall.

The deep sea is the lowest layer in the ocean. As no sunlight reaches such a depth, most of the deep-sea region is dark, quiet, and chilling. The ambient temperature in the deep sea environment measures 2-4 ℃ only [1]. In contrast to the barrenness in the majority of the deep sea, the area around hydrothermal vent fields, a fissure on the seafloor from which geothermally heated water discharges, is biologically more thriving, often hosting complex communities fueled by the chemicals dissolved in the vent fluids (Fig. 1a). The water temperature near the hydrothermal vents fluctuates, depending on the geological activity of the vent and the distance from the vent exit. The temperature at the exit of a hydrothermal vent can reach up to 300-400 ℃ and drops quickly to the ambient temperature as the discharged hot water mixes with the chilling seawater surrounding [2]. For the animals inhabiting the vicinity of the hydrothermal vents especially those with less locomobility, selection of a proper distance from their dwelling to the vent is tricky. Proximity to the vent certainly brings ease for acquiring food and nutrient but meanwhile causes a higher risk of experiencing thermal impulses from the hot flow. Deep-sea explorations unveiled that there are diverse species of gastropods inhabiting near the deep-sea hydrothermal vents. Among them, the most intriguing one might be the snail of *Chrysomallon squamiferum*, which is well-known for its unique scales on the dorsal side of the foot and was discovered in different vent fields in the Indian Ocean such as the Kairei field [3, 4], Longqi field [5-7], and Tiancheng field [8]. The sedentary life of these hydrothermal-vent snails in combination with the unstable temperature in their habitat implies the high possibility of having an effective design strategy in their exoskeletal shells for tackling the thermal impulses [3]. Simple structural characterizations indicated a common structural feature in the shells of hydrothermal-vent snails. That is, a monolithic and relatively thick, organic periostracum layer is deployed outside the inorganic calcium carbonate layer. For example, in the shell of a snail *C. squamiferum* collected from the Longqi field, the organic periostracum layer accounts for ~40-50 % of the total shell thickness, as shown in Fig. 1b. A similar bi-layer structure was also reported in the shell of *Alviniconcha hessleri* [9], another species of gastropod living near the deep-sea hydrothermal vent. Such a thick and monolithic organic layer is not common in the shells of the land snails and marine gastropods in shallow water, in which the periostracum layer, if available, is much thinner as compared to the inner mineralized layer [10]. To verify whether such a unique design in the shells of the hydrothermal-vent snails would bring about any unusual thermal property, temperature evolution on one side of the shell of a scaly-foot snail (*C. squamiferum*) in response to a high-temperature impulse applied on the opposite side is measured (see Materials and methodology). Fig. 1c shows that when a thermal impulse of temperature ~88 ℃ and duration of ~11 s is applied on the outer wall (OW) of the shell of the snail *C. squamiferum*, the peak temperature measured on the inner wall (IW) reaches ~63 ℃. In contrast, if a thermal impulse with the same temperature and duration is applied on the IW, the peak temperature measured on the OW reaches as high as ~83 ℃, implying the significant efficacy of the snail shell in resisting the external thermal impulse. To further reveal the mechanism accounting for the higher thermal resistance exhibited by the shell of hydrothermal-vent snails, a theoretical model is established to investigate the temperature response of a bilayer structure to an external thermal impulse with the focus on its dependence on the structural attributes such as the layout sequence and thickness of the composing layers. The results obtained from this model can also provide useful guidelines for the design and optimization of the thermal barrier coatings aiming at higher thermal impulse resistance [11-13].

THEORETICAL MODELING

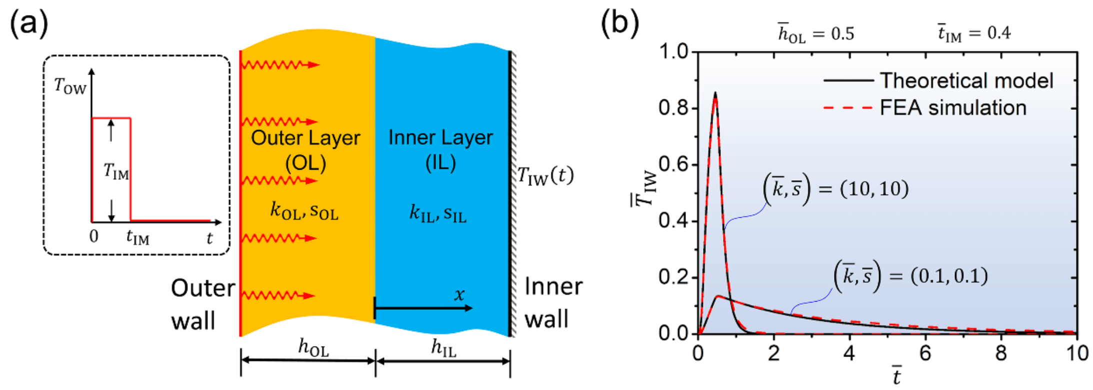

Fig. 2 (**a**) Schematic depiction of 1-D thermal conduction model of a bilayer subjected to a thermal impulse. (**b**) Comparisons between the temperature responses on the inner wall, $\overline{T}_{IW}$, obtained by theoretical model and finite element analysis (FEA).

Consider a bilayer structure composed of the outer layer (OL) and the inner layer (IL) with dissimilar thicknesses (h), thermal conductivities (k), and volumetric heat capacities (s), as shown in Fig. 2a. Initially, the whole system is at the temperature T_0. At $t = 0$, an instant temperature increment of T_{IM} is applied on the outer wall of the bilayer and lasts for a period of t_{IM}, simulating the impact of an instantaneous thermal impulse. The inner wall of the bilayer is assumed thermally insulative and the thermal resistance of the interface between the OL and IL is neglected for the moment. The time-dependent temperature field in the bilayer, which is denoted by $T(x, t)$, should satisfy the governing equations of thermal conductivity as follows

$$\begin{cases} \dfrac{\partial T}{\partial t} = \dfrac{k_{OL}}{s_{OL}} \dfrac{\partial^2 T}{\partial x^2}, & (-h_{OL} < x < 0) \\ \dfrac{\partial T}{\partial t} = \dfrac{k_{IL}}{s_{IL}} \dfrac{\partial^2 T}{\partial x^2}, & (0 < x < h_{IL}) \end{cases} \tag{1}$$

where $k_{OL(IL)}$ and $s_{OL(IL)}$ stand for the materials' *thermal conductivities* and *volumetric heat capacities* of the OL and IL, respectively.

Introducing dimensionless parameters

$$\overline{T} \equiv \frac{T - T_0}{T_{IM}}, \quad \overline{x} \equiv \frac{x}{h_{OL} + h_{IL}}, \quad \overline{t} \equiv \frac{t}{(h_{OL} + h_{IL})^2} \sqrt{\frac{k_{OL} k_{IL}}{s_{OL} s_{IL}}},$$
$$\overline{k} \equiv \frac{k_{OL}}{k_{IL}}, \quad \overline{s} \equiv \frac{s_{OL}}{s_{IL}}, \quad \overline{h}_{OL(IL)} \equiv \frac{h_{OL(IL)}}{h_{OL} + h_{IL}} \tag{2}$$

Eq. (1) can be rewritten in a normalized form as

$$\begin{cases} \dfrac{\partial \overline{T}}{\partial \overline{t}} = \sqrt{\dfrac{\overline{k}}{\overline{s}}} \dfrac{\partial^2 \overline{T}}{\partial \overline{x}^2}, & (-\overline{h}_{OL} < \overline{x} < 0) \\ \dfrac{\partial \overline{T}}{\partial \overline{t}} = \sqrt{\dfrac{\overline{s}}{\overline{k}}} \dfrac{\partial^2 \overline{T}}{\partial \overline{x}^2}, & (0 < \overline{x} < \overline{h}_{IL}) \end{cases} \tag{3}$$

The initial condition and boundary conditions can be given in a normalized form as

$$\bar{T}(\bar{x},0)=0,\ \bar{T}(-\bar{h}_{\mathrm{OL}},\bar{t})=1-\mathrm{H}(\bar{t}-\bar{t}_{\mathrm{IM}}),\ \frac{\partial\bar{T}(\bar{h}_{\mathrm{IL}},\bar{t})}{\partial\bar{x}}=0 \tag{4}$$

where $\bar{t}_{\mathrm{IM}}\equiv\frac{t_{\mathrm{IM}}}{(h_{\mathrm{OL}}+h_{\mathrm{IL}})^2}\sqrt{\frac{k_{\mathrm{OL}}k_{\mathrm{IL}}}{s_{\mathrm{OL}}s_{\mathrm{IL}}}}$ is the normalized duration of the thermal impulse, and $\mathrm{H}(\bar{t}-\bar{t}_{\mathrm{IM}})$ stands for a unit step function taking 0 when $\bar{t}<\bar{t}_{\mathrm{IM}}$ and 1 when $\bar{t}\geq\bar{t}_{\mathrm{IM}}$.

The continuity of temperature and conservation of heat flux across the interface between the OL and IL ($x=0$) require that

$$\bar{T}(0^-,\bar{t})=\bar{T}(0^+,\bar{t}),\ \bar{k}\frac{\partial\bar{T}(0^-,\bar{t})}{\partial\bar{x}}=\frac{\partial\bar{T}(0^+,\bar{t})}{\partial\bar{x}} \tag{5}$$

To solve the above partial differential equations (PDEs) about $\bar{T}(\bar{x},\bar{t})$, Laplace transformation is applied to Eqs. (3-5). Then the governing equations are converted into ordinary differential equations (ODEs) as follows:

$$\begin{cases}\dfrac{\partial^2 U}{\partial\bar{x}^2}-p\sqrt{\dfrac{\bar{s}}{\bar{k}}}U=0, & (-\bar{h}_{\mathrm{OL}}<\bar{x}<0)\\[2ex] \dfrac{\partial^2 U}{\partial\bar{x}^2}-p\sqrt{\dfrac{\bar{k}}{\bar{s}}}U=0, & (0<\bar{x}<\bar{h}_{\mathrm{IL}})\end{cases} \tag{6}$$

where function $U(\bar{x},p)$ is the Laplace transform of the function $\bar{T}(\bar{x},\bar{t})$, namely $U(\bar{x},p)=\mathcal{L}[\bar{T}(\bar{x},\bar{t})]=\int_0^\infty\bar{T}(\bar{x},\bar{t})e^{-p\bar{t}}d\bar{t}$. The corresponding boundary conditions and continuity requirements are also mapped to the complex domain as

$$U(-\bar{h}_{\mathrm{OL}},p)=\frac{1}{p}(1-e^{-\bar{t}_{\mathrm{IM}}p}),\ \frac{\partial U(\bar{h}_{\mathrm{IL}},p)}{\partial\bar{x}}=0 \tag{7}$$

$$U(0^-,p)=U(0^+,p),\ \bar{k}\frac{\partial U(0^-,\bar{t})}{\partial\bar{x}}=\frac{\partial U(0^+,\bar{t})}{\partial\bar{x}} \tag{8}$$

Solving Eq. (6) in combination with the conditions given by Eqs. (7-8) for function $U(\bar{x},p)$ and then taking the inverse Laplace transform give rise to the solution to $\bar{T}(\bar{x},\bar{t})$ as

$$\bar{T}=\begin{cases}\mathcal{L}^{-1}\left[\dfrac{2(1-e^{-\bar{t}_{\mathrm{IM}}p})\left(m_1m_2+m_3m_4\sqrt{\bar{k}\bar{s}}-m_4F\sqrt{\bar{k}\bar{s}}\right)}{p\left(m_1^2m_2+m_1m_3m_4\sqrt{\bar{k}\bar{s}}\right)}\right], & (-\bar{h}_{\mathrm{OL}}<\bar{x}<0)\\[3ex] \mathcal{L}^{-1}\left[\dfrac{2\sqrt{\bar{k}\bar{s}}(1-e^{-\bar{t}_{\mathrm{IM}}p})G}{p\left(m_1m_2\sqrt{\bar{k}\bar{s}}+m_3m_4\right)}\right], & (0<\bar{x}<\bar{h}_{\mathrm{IL}})\end{cases} \tag{9}$$

where

$$\begin{cases} m_1 = 2\cosh\left(\bar{h}_{\mathrm{OL}}\sqrt{p\sqrt{\bar{s}/\bar{k}}}\right) \\ m_2 = 2\cosh\left(\bar{h}_{\mathrm{IL}}\sqrt{p\sqrt{\bar{k}/\bar{s}}}\right) \\ m_3 = 2\sinh\left(\bar{h}_{\mathrm{OL}}\sqrt{p\sqrt{\bar{s}/\bar{k}}}\right) \\ m_4 = 2\sinh\left(\bar{h}_{\mathrm{IL}}\sqrt{p\sqrt{\bar{k}/\bar{s}}}\right) \end{cases} \tag{10}$$

and functions F and G are given by

$$\begin{cases} F = 2\sinh\left((\bar{x} + \bar{h}_{\mathrm{OL}})\sqrt{p\sqrt{\bar{s}/\bar{k}}}\right) \\ G = 2\cosh\left((\bar{x} - \bar{h}_{\mathrm{IL}})\sqrt{p\sqrt{\bar{k}/\bar{s}}}\right) \end{cases} \tag{11}$$

The temperature on the inner wall ($x = h_{\mathrm{IL}}$) of the bilayer, denoted as $\bar{T}_{\mathrm{IW}}$, thus is given by

$$\bar{T}_{\mathrm{IW}}(\bar{t}) = \bar{T}(\bar{x} = \bar{h}_{\mathrm{IL}}, \bar{t}) = \mathcal{L}^{-1}\left[\frac{4\sqrt{\bar{k}\bar{s}}\left(1 - e^{-\bar{t}_{\mathrm{IM}}p}\right)}{p\left(m_1 m_2\sqrt{\bar{k}\bar{s}} + m_3 m_4\right)}\right] \tag{12}$$

Given $\bar{k}$, $\bar{s}$, $\bar{t}_{\mathrm{IM}}$, and $\bar{h}_{\mathrm{OL(IL)}}$, the temperature $\bar{T}_{\mathrm{IW}}$ at any moment of time $\bar{t}$ can be calculated numerically from Eq. (12) (MATLAB, The MathWorks, Inc.), giving rise to the numerical solution to the temporal evolution of $\bar{T}_{\mathrm{IW}}(\bar{t})$. To verify the results obtained from the bilayer model, finite element analysis (FEA) (ABAQUS, Dassault Systèmes) is carried out. The evolutions of $\bar{T}_{\mathrm{IW}}$ with $\bar{t}$ obtained by the bilayer model agree well with the FEA results (see Fig. 2b). The analytical solution given by Eq. (12) is verified.

It should be pointed out that, in the above bilayer model, the interfacial thermal resistance between the OL and IL is ignored, and the inner wall of the IL is assumed thermally insulating. The effects of interfacial thermal resistance and possible heat flux crossing the inner wall are investigated and found to play insignificant roles in determining the temperature response on the inner wall of the snail shell (see online **Supplementary Material**). Therefore, the simplified bilayer model will be applied below to study the thermal resistance of the shell to thermal impulse.

RESULTS AND DISCUSSIONS

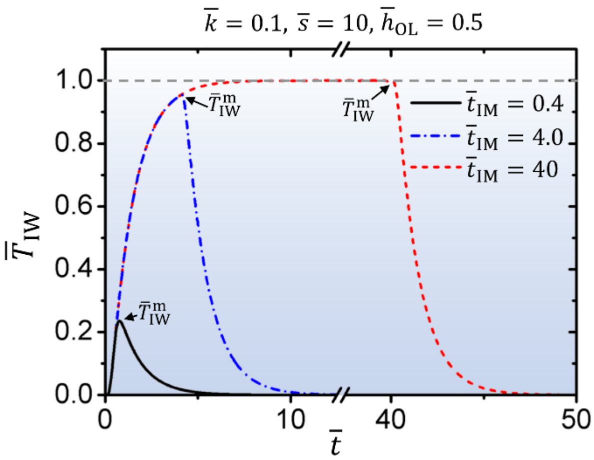

Fig. 3 Calculated evolution of the temperature on the inner wall, $\bar{T}_{\mathrm{IW}}$, with the time $\bar{t}$ in response to the external thermal impulse with periods $\bar{t}_{\mathrm{IM}} = 0.4$, 4, and 40, respectively. As an example, here the ratios of the thermal conductivity and volumetric heat capacity between two layers are assumed as $\bar{k} = 0.1$ and $\bar{s} = 10$, respectively, and the thickness of the IL and OL are assumed the same (*i.e.*, $\bar{h}_{\mathrm{OL}} = 0.5$).

Taking $\bar{k} = 0.1$, $\bar{s} = 10$, $\bar{h}_{\mathrm{OL}} = 0.5$, Fig. 3 shows the calculated evolution of $\bar{T}_{\mathrm{IW}}$ in response to thermal impulses with different durations of $\bar{t}_{\mathrm{IM}} = 0.4, 4, 40$. One can see that $\bar{T}_{\mathrm{IW}}$ exhibits a similar trend of evolution. At $\bar{t} = 0$ when the external impulse is applied, it starts to grow until a moment shortly after the cease of the thermal impulse at $\bar{t} = \bar{t}_{\mathrm{IM}}$. After that, $\bar{T}_{\mathrm{IW}}$ declines gradually to zero as time goes by. The apex of the $\bar{T}_{\mathrm{IW}}$, which is denoted by $\bar{T}_{\mathrm{IW}}^{\mathrm{m}}$, is indicated in Fig. 3 for each studied case. If the impulse lasts shortly, $\bar{T}_{\mathrm{IW}}^{\mathrm{m}}$ could be much lower than the temperature applied on the outer wall, implying the considerable resistance to the thermal impulse of the bilayer. The magnitude of $\bar{T}_{\mathrm{IW}}^{\mathrm{m}}$ is applied to quantify the resistance of the bilayer to a thermal impulse. The lower the $\bar{T}_{\mathrm{IW}}^{\mathrm{m}}$, the higher the thermal resistance. Recalling the definition of the normalized time in Eq. (2), one can see that $\bar{t}_{\mathrm{IM}}$ is proportional not only to the impulse duration (t_{IM}), but also to the geometric mean of the thermal diffusivities (*i.e.*, k/s) of two layers and inversely proportional to $(h_{\mathrm{OL}} + h_{\mathrm{IL}})^2$. This agrees well with our common sense that using materials with lower thermal diffusivities or increasing the overall thickness of the bilayer will also lead to lower $\bar{t}_{\mathrm{IM}}$ and therefore benefits the thermal impulse resistance. Nevertheless, given the building materials and overall thickness of the bilayer, how can we maximize its resistance to thermal impulse remains unclear. To answer this question, the effects of layer sequence and volume (thickness) fraction on thermal resistance should be investigated as follows.

Effect of layer sequence on the resistance to thermal impulse

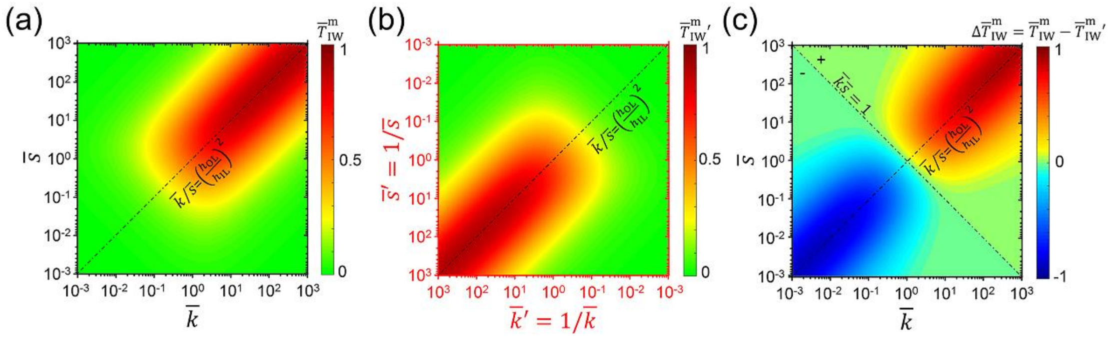

Fig. 4 (**a**) Contour plot of the peak temperature on the IW ($\overline{T}_{\rm IW}^{\rm m}$) with $\bar{k}$ and $\bar{s}$ in the range of $[10^{-3}, 10^{3}]$. (**b**) Contour plot of the peak temperature on the IW of the bilayers with a swapped layer sequence ($\overline{T}_{\rm IW}^{\rm m}{}'$). (**c**) Contour plot of the difference between $\overline{T}_{\rm IW}^{\rm m}$ and $\overline{T}_{\rm IW}^{\rm m}{}'$. Here, $\bar{h}_{\rm OL} = 0.5$ and $\bar{t}_{\rm IM} = 0.4$.

The first factor we would like to investigate is the layout sequence of two layers in the bilayer. Based on the temperature response on the IW as given in Eq. (12), Fig. 4a shows the contour of $\overline{T}_{\rm IW}^{\rm m}$ on the $\bar{k}$-$\bar{s}$ plane (logarithmic scale) in the domain of $\bar{k} \in [10^{-3}, 10^{3}]$ and $\bar{s} \in [10^{-3}, 10^{3}]$. For the moment, it is assumed that the OL and IL have the same thickness, namely, $\bar{h}_{\rm OL} = 0.5$. It can be seen that the contour of $\overline{T}_{\rm IW}^{\rm m}$ is symmetric about the line of $\bar{k} = \bar{s}\left(\frac{\bar{h}_{\rm OL}}{\bar{h}_{\rm IL}}\right)^2$ (see online **Supplementary Material** for a rigorous demonstration). Elevated $\overline{T}_{\rm IW}^{\rm m}$ occurs as $\bar{k}$ and $\bar{s}$ grow along the line of symmetry. This is the scenario that one should avoid when designing a bilayer for resisting the thermal impulse. The simplest way to reduce $\overline{T}_{\rm IW}^{\rm m}$ is to swap the layout sequence of the OL and IL. To evaluate the effect of swapping layer sequence on the thermal impulse resistance, the maximum temperature on the inner wall of a bilayer with swapped layer sequence, which is denoted by $\overline{T}_{\rm IW}^{\rm m}{}'$, is plotted in Fig. 4b. The difference between $\overline{T}_{\rm IW}^{\rm m}$ and $\overline{T}_{\rm IW}^{\rm m}{}'$, which is denoted as $\Delta\overline{T}_{\rm IW}^{\rm m}$, then is plotted in Fig. 4c, showing the effect of layer sequence on the thermal impulse resistance. It can be seen that $\Delta\overline{T}_{\rm IW}^{\rm m}$ is negative when $\bar{k}\bar{s} < 1$ and positive when $\bar{k}\bar{s} > 1$. This implies that for higher thermal impulse resistance two layers should be placed in such a sequence that the product of $\bar{k}$ and $\bar{s}$ is less than 1. Fig. 4c also indicates that for bilayers with $\bar{k}\bar{s} = 1$, $\overline{T}_{\rm IW}^{\rm m}$ is insensitive to the layer sequence. This can be theoretically attributed to the intrinsic exchangeability of $\bar{h}_{\rm IL}^{-2}\bar{k}$ and $\bar{h}_{\rm OL}^{-2}\bar{s}$ in the function of $\overline{T}_{\rm IW}$. That is, the contour of $\overline{T}_{\rm IW}^{\rm m}$ is symmetric about the line of $\bar{k} = \bar{s}\left(\frac{\bar{h}_{\rm OL}}{\bar{h}_{\rm IL}}\right)^2$.

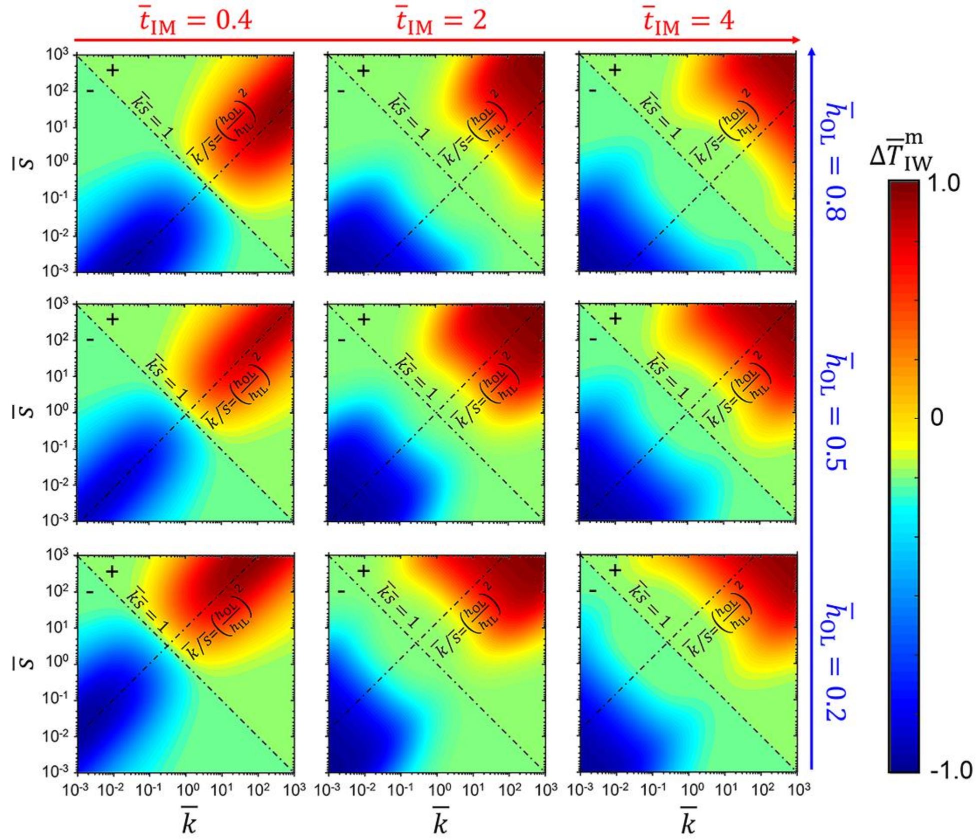

Fig. 5. Contour plots of the change of peak temperature on IW after swapping the layer sequence ($\bar{T}_{\mathrm{IW}}^{\mathrm{m}} - \bar{T}_{\mathrm{IW}}^{\mathrm{m}\,\prime}$) for $\bar{h}_{\mathrm{OL}} = 0.2, 0.5, 0.8$ and $\bar{t}_{\mathrm{IM}} = 0.4, 2, 4$.

The above discussion can be further extended to the bilayers with dissimilar thickness ratios between the OL and IL. Fig. 5 shows the contour plots of $\Delta\bar{T}_{\mathrm{IW}}^{\mathrm{m}}$ for bilayers with $\bar{h}_{\mathrm{OL}} = 0.2, 0.5, 0.8$. Evidently, $\Delta\bar{T}_{\mathrm{IW}}^{\mathrm{m}}$ is negative when $\bar{k}\bar{s} < 1$, irrespective of the values of $\bar{h}_{\mathrm{OL}}$. It is also found from Fig. 5 that the layer sequence leading to better thermal impulse resistance does not depend on $\bar{t}_{\mathrm{IM}}$. Moreover, Fig. 5 indicates that varying $\bar{h}_{\mathrm{OL}}$ causes a translation of the contour of $\Delta\bar{T}_{\mathrm{IW}}^{\mathrm{m}}$ on the $\bar{k}$-$\bar{s}$ plane. This implies that the thermal impulse resistance of a bilayer can be further optimized by tuning $\bar{h}_{\mathrm{OL}}$, as elaborated next.

Effect of volume (thickness) fraction on the resistance to thermal impulse

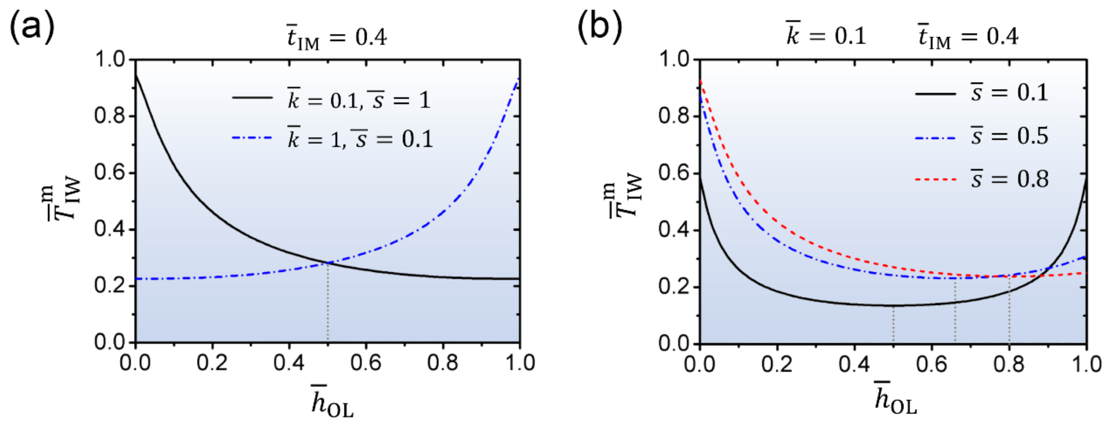

Fig. 6 The dependence of the maximum temperature experienced by the inner wall ($\bar{T}_{\mathrm{IW}}^{\mathrm{m}}$) on the thickness fraction of the OL ($\bar{h}_{\mathrm{OL}}$) for (**a**) $\bar{k} = 0.1$, $\bar{s} = 1$ and $\bar{k} = 1$, $\bar{s} = 0.1$, and (**b**) $\bar{k} = 0.1$, $\bar{s} = 0.1, 0.5, 0.8$, respectively.

Having determined the optimal layer sequence, the remaining variable one can tune for higher thermal impulse resistance is the volume fractions of two materials, which are equivalent to the thickness fractions $\bar{h}_{\mathrm{OL(IL)}}$ in our bilayer model. Consider a bilayer with optimal layer sequence, namely, $\bar{k}\bar{s} < 1$. If $\bar{k} < 1$ and $\bar{s} \geq 1$, the OL has lower thermal conductivity but higher volumetric heat capacity than the IL does. Under this circumstance, having thicker OL and thinner IL benefits the thermal impulse resistance of the bilayer provided that the total thickness is fixed. Therefore, $\bar{T}_{\mathrm{IW}}^{\mathrm{m}}$ monotonically decreases as $\bar{h}_{\mathrm{OL}}$ increases from 0 to 1. In contrast, if $\bar{k} \geq 1$ and $\bar{s} < 1$, the OL has higher thermal conductivity but lower volumetric heat capacity than the IL does. $\bar{T}_{\mathrm{IW}}^{\mathrm{m}}$ monotonically increases with $\bar{h}_{\mathrm{OL}}$. Under this circumstance, the thinner the OL the higher the thermal impulse resistance of the bilayer. To illustrate the dependence of thermal impulse resistance on the thickness fractions in these two cases, we plot the variation of $\bar{T}_{\mathrm{IW}}^{\mathrm{m}}$ with $\bar{h}_{\mathrm{OL}}$ by taking $\bar{k} = 0.1$, $\bar{s} = 1$ and $\bar{k} = 1$, $\bar{s} = 0.1$, as shown in Fig. 6a.

In addition to the above two scenarios, it might be also possible to have a bilayer in which the OL is inferior in both thermal conductivity and volumetric heat capacity compared with the IL, namely $\bar{k} < 1$ and $\bar{s} < 1$. Under this circumstance, $\bar{T}_{\mathrm{IW}}^{\mathrm{m}}$ does not exhibit a monotonic dependence on $\bar{h}_{\mathrm{OL}}$ due to the opposite effects of thermal conductivity and heat capacity on the resistance to thermal impulse. Instead, there exists an optimal $\bar{h}_{\mathrm{OL}}$, at which $\bar{T}_{\mathrm{IW}}^{\mathrm{m}}$ is minimized, as illustrated by Fig. 6b. Therefore, the thermal impulse resistance of the bilayer can be maximized by adopting the optimal $\bar{h}_{\mathrm{OL}}$, which is dependent on the values of $\bar{k}$ and $\bar{s}$. Since the limiting cases with $\bar{h}_{\mathrm{OL}} = 0$ and $\bar{h}_{\mathrm{OL}} = 1.0$ in Fig. 6b represent two single-layered structures with materials being that of the IL and OL respectively, Fig. 6b indicates that the bilayer structure with $\bar{k} < 1$ and $\bar{s} < 1$ always exhibits superior resistance to thermal impulse compared with the corresponding single-layered counterparts of the same thickness. Recall the multilayer design of the snail shells from the hydrothermal environment. It is of great interest to verify whether the hydrothermal-vent snails have adopted such an optimal design in their shells for higher thermal impulse resistance.

Snail shells from the hydrothermal environment: Optimal design for higher thermal impulse resistance in nature

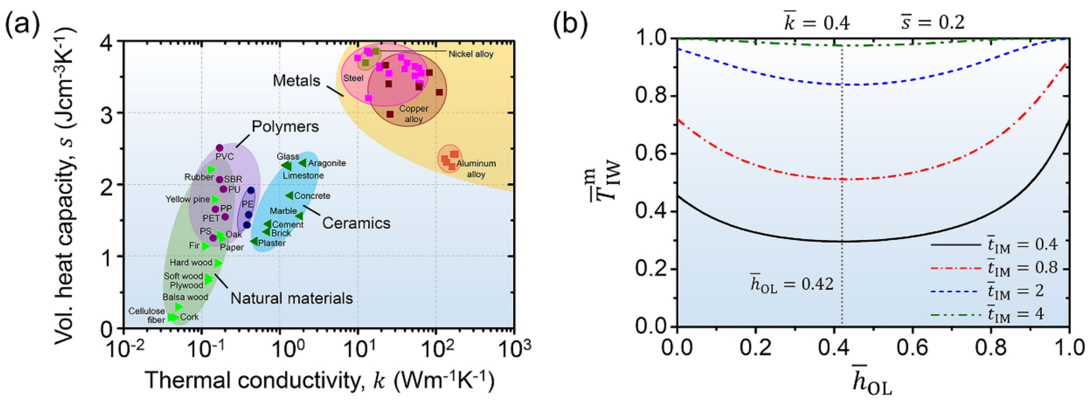

Fig. 7 (**a**) Ashby diagram of thermal conductivity versus volumetric heat capacity for typical structural and heat-resistant engineering materials [14-19]. (**b**) Calculated variations of $\bar{T}_{IW}^{m}$ with $\bar{h}_{OL}$ in response to the external thermal impulse with periods $\bar{t}_{IM} = 0.4$, 0.8, 2, and 4, respectively. The OL is assumed as organic material with $k = 0.8$ W m^{-1}K^{-1}and $s = 0.46$ J cm^{-3}K^{-1}, and the IL is assumed as inorganic material with $k = 2.0$ W m^{-1}K^{-1} and $s = 2.3$ J cm^{-3}K^{-1}.

In our preceding discussion, we have not considered the ranges of thermal conductivity (k) and volumetric heat capacity (s) of the available materials. Actually, k and s of materials vary in different ranges, as shown by the k-s Ashby plot in Fig. 7a. It can be seen that k spans three orders of magnitude from 10^{-1} to 10^{2} W m^{-1}K^{-1}, while s ranges only from 0.1 to 4 J cm^{-3}K^{-1}. For the gastropods in nature, the materials available for constructing their exoskeletal shells are limited, including calcified ceramics and organic materials. For example, most seashells are composed of calcium carbonate, typically aragonite, and protein-based organic materials. Given these two kinds of materials, how can we design a bilayer with higher thermal impulse resistance?

For aragonite, the typical values of thermal conductivity and volumetric heat capacity are around 2.0 W m^{-1}K^{-1} [18] and 2.3 J cm^{-3}K^{-1} [19], respectively. On the other hand, for the organic phase like protein, chitin, and other biomacromolecule matters, the typical values of k and s are around 0.8 W m^{-1}K^{-1} [20] and 0.46 J cm^{-3}K^{-1} [21, 22], respectively, which approximately lie in the ranges of natural materials in the Ashby plot (Fig. 7a). Apparently, the organic phase is inferior in both thermal conductivity and heat capacity in comparison to the calcified ceramic phase. According to our result in Section 3.1, the organic phase should be placed outside of the ceramic phase in order to achieve a higher resistance to thermal impulse, resulting in a bilayer with $\bar{k} = 0.4$ and $\bar{s} = 0.2$. For such a bilayer, the thermal impulse resistance can be further optimized by tuning the thickness fraction $\bar{h}_{\mathrm{OL}}$ since $\bar{k} < 1$ and $\bar{s} < 1$ as indicated in Section 3.2. The calculated $\bar{T}_{\mathrm{IW}}^{\mathrm{m}}$ caused by different thermal impulses is plotted in Fig. 7b as a function of $\bar{h}_{\mathrm{OL}}$. Here, different impulse durations $\bar{t}_{\mathrm{IM}} = 0.4, 0.8, 2$ and 4 are considered with corresponding actual time durations being 0.1 s, 0.2 s, 0.5 s and 1 s, respectively, as estimated according to the reported information of the material compositions and the thickness of the snail shells [3]. From Fig. 7b, the optimal thickness fraction is estimated to be $\bar{h}_{\mathrm{OL}} \approx 0.42$, irrespective of the duration of the thermal impulse. This result is consistent with the thickness fraction of the periostracum layer observed in the shell of *C. squamiferum* (~40-50 %) (see Fig. 1b). Such an optimized design of the exoskeletal shell might be the consequence of evolutionary adaption as it can greatly enhance the survival rate of the snails in the extreme thermal environment near the deep-sea hydrothermal vents.

For engineering structures with more than two material layers, the temperature evolution in response to the external thermal impulse is mathematically difficult to be solved. However, the above results obtained from the bilayer model can be adopted to design and optimize the thermal impulse resistance of a multilayered structure. First, one can choose two materials to design a bilayer with optimal thermal impulse resistance based on the results obtained from this study, then replace the bilayer with an equivalent homogeneous single layer with the same thermal properties [23-25]. Such equivalent single layer can be further assembled with the next material layer to form a new bilayer, followed by structural optimization for higher thermal resistance. By repeating such a process, we can obtain the multilayered structure with the best thermal impulse resistance.

CONCLUSIONS

In this paper, we theoretically studied the effect of structural determining factors, including layer sequence and volume fraction, on the thermal impulse resistance of a bilayer to the external thermal impulse. Based on our results, two practical guidelines of the layout design of bilayer structures for higher resistance to thermal impulse are proposed as follows:

1. For two layers with distinct thermal properties, their layout sequence plays an important role in determining the overall thermal impulse resistance of the bilayer. For higher resistance to the thermal impulse of the bilayer, one should place the two layers in such a sequence that the product of the conductivity ratio and volumetric capacity ratio between the OL and IL is less than 1, namely, $\frac{k_{\mathrm{OL}}}{k_{\mathrm{IL}}}\frac{s_{\mathrm{OL}}}{s_{\mathrm{IL}}} < 1$.
2. For a bilayer with an optimized layer sequence, the thermal impulse resistance can be further optimized by tuning the thickness fraction of the layers. If $\frac{k_{\mathrm{OL}}}{k_{\mathrm{IL}}} < 1$ and $\frac{s_{\mathrm{OL}}}{s_{\mathrm{IL}}} \geq 1$(or, alternatively $\frac{k_{\mathrm{OL}}}{k_{\mathrm{IL}}} \geq 1$ and $\frac{s_{\mathrm{OL}}}{s_{\mathrm{IL}}} < 1$), thicker OL (or IL) leads to the higher thermal impulse resistance of the bilayer. If $\frac{k_{\mathrm{OL}}}{k_{\mathrm{IL}}} < 1$ and $\frac{s_{\mathrm{OL}}}{s_{\mathrm{IL}}} < 1$, there exist optimal thickness fractions, at which the thermal impulse resistance of the bilayer is maximized.

Our findings not only account for the success of the deep-sea snails in surviving the thermal impulses from the hydrothermal vents but also provide a theoretical basis and operational guidelines for the design and optimization of thermal barriers in engineering.

MATERIALS AND METHODOLOGY

Sample collection of the shells of scaly-foot snails

Scaly-foot snails (*C. squamiferum*) were collected from Longqi (37.7839°S, 49.6502°E; 2,761 m depth) vent field with the suction sampler on the ROV Sea Dragon III. These samples were stored in -80℃ deep freezer until further usage. The snails were dissected in the lab. The shells were bleached with NaOCl solution (0.26% active chlorine) for 3 hours, further cleaned with distilled water and dried.

Characterization of the thermal resistance of snail shells to a thermal impulse

A small homemade hot-water fountain was developed to produce a heat source with a constant temperature. The water temperature at the fountain spout ($\sim$1.0 mm in diameter) was monitored using a thermocouple thermometer to ensure that it was always kept in the range of 88 ± 1 ℃ during the experiments. The thermal impulse was applied on one side of the snail shell (either OW or IW) by placing the shell quickly on the top of the fountain stream and holding for 10 s. During the experiments, the distance between the shell and the fountain spout and the orientation of the shell were controlled with caution to avoid the splash of hot water onto the opposite side, where the temperature evolution was measured and recorded using a thermocouple thermometer attached.

Finite element verification of the bilayer model

The temperature evolution on the inner wall (IW) of the laminated shell in response to a thermal impulse applied on the outer wall (OW) was simulated as a transient thermal conduction problem using finite element method (ABAQUS, Dassault Systèmes). 8-node heat transfer brick elements (DC3D8) were adopted in all simulations. The initial temperature of the whole simulation system was set as T_0. At the beginning of simulations, the temperature on the OW of the shell was instantly increased by a specified value (T_{IM}). After a specified period (t_{IM}), the temperature on the OW was set back to the initial value (T_0). The thicknesses ($h_{\mathrm{OL}}, h_{\mathrm{IL}}$) and the thermal properties ($k_{\mathrm{OL}}, k_{\mathrm{IL}}, s_{\mathrm{OL}}, s_{\mathrm{IL}}$) of each layer, and the duration of the applied thermal impulse (t_{IM}) were taken in such a way that the resulting $\bar{h}_{\mathrm{OL}}$, $\bar{k}$, $\bar{s}$ and $\bar{t}_{\mathrm{IM}}$ consist with those adopted in the theoretical bilayer model for comparison. All the boundaries except the OW were assumed thermally insulating. Thermal resistance on the interface between two layers was neglected in the simulations. Based on the calculated evolution of temperature on the IW (T_{IW}) with the time (t), the evolution of the normalized temperature $\bar{T}_{\mathrm{IW}} \equiv \frac{T_{\mathrm{IW}}-T_0}{T_{\mathrm{IM}}}$ with the normalized time $\bar{t} \equiv \frac{t}{(h_{\mathrm{OL}}+h_{\mathrm{IL}})^2}\sqrt{\frac{k_{\mathrm{OL}}k_{\mathrm{IL}}}{s_{\mathrm{OL}}s_{\mathrm{IL}}}}$ was obtained.

ACKNOWLEDGEMENT

This work was supported by the Research Grant Council of Hong Kong (Grant No.: PolyU152064/15E) and the General Research Fund of Hong Kong Polytechnic University (G-UAHN). We are grateful to the technical support of the crew member of *Dayangyihao* and pilots of ROV *Sea Dragon III* during the cruise of COMRA DY52nd.

CONFLICT OF INTEREST

On behalf of all authors, the corresponding author declares that there is no conflict of interest.

SUPPLEMENTARY MATERIAL

The online version of this article (https://doi.org/xxxx) contains supplementary materials, with is available to authorized users.

REFERENCES

[1] A. Maruyama, R. Taniguchi, H. Tanaka, H. Ishiwata, and T. Higashihara, *Mar. Biol.* 128, 705 (1997).

[2] K. Ding, W.E. Seyfried Jr, M. Tivey, and A. Bradley, *Earth Planet. Sci. Lett.* 186, 417 (2001).

[3] H. Yao, M. Dao, T. Imholt, J. Huang, K. Wheeler, A. Bonilla, S. Suresh, and C. Ortiz, *Proc. Natl. Acad. Sci. U. S. A.* 107, 987 (2010).

[4] J. Sun, C. Chen, N. Miyamoto, R. Li, J.D. Sigwart, T. Xu, Y. Sun, W.C. Wong, J.C.H. Ip, W. Zhang, Y. Lan, D. Bissessur, T.-o. Watsuji, H.K. Watanabe, Y. Takaki, K. Ikeo, N. Fujii, K. Yoshitake, J.-W. Qiu, K. Takai, and P.-Y. Qian, *Nat. Commun.* 11, 1657 (2020).

[5] C. Tao, J. Lin, S. Guo, Y.J. Chen, G. Wu, X. Han, C.R. German, D.R. Yoerger, N. Zhou, H. Li, X. Su, and J. Zhu, *Geology* 40 47 (2012).

[6] Y. Zhou, D. Zhang, R. Zhang, Z. Liu, C. Tao, B. Lu, D. Sun, P. Xu, R. Lin, J.j. Wang, and C. Wang, *Deep Sea Res., Part I* 137, 1 (2018).

[7] C. Chen, K. Linse, J.T. Copley, and A.D. Rogers, *J. Molluscan Stud.* 81, 322 (2015).

[8] J. Sun, Y. Zhou, C. Chen, Y.H. Kwan, Y. Sun, X. Wang, L. Yang, R. Zhang, T. Wei, Y. Yang, L. Qu, C. Sun, and P.-Y. Qian, *R. Soc. Open Sci.* 7, 200110 (2020).

[9] T. Okutani and S. Ohta, *Venus (Jap. J. Malacology)* 47, 1 (1988).

[10] A. Checa, *Tissue Cell* 32, 405 (2000).

[11] R. Vaßen, M.O. Jarligo, T. Steinke, D.E. Mack, and D. Stöver, *Surf. Coat. Technol.* 205, 938 (2010).

[12] V. Viswanathan, G. Dwivedi, and S. Sampath, *J. Am. Ceram. Soc.* 97, 2770 (2014).

[13] V. Viswanathan, G. Dwivedi, and S. Sampath, *J. Am. Ceram. Soc.* 98, 1769 (2015).

[14] C.A. Harper, *Handbook of building materials for fire protection*, (New York, McGraw-Hill, 2004).

[15] H.L. John IV and H.L. John V, *A heat transfer textbook*, (Cambridge, Massachusetts, U.S.A, Phlogiston Press, 2019), pp. 714-735.

[16] T.L. Bergman, F.P. Incropera, D.P. DeWitt, and A.S. Lavine, *Fundamentals of heat and mass transfer*, (Hoboken, NJ, John Wiley & Sons, 2011), pp. 981-1012.

[17] P.J. DiNenno, D. Drysdale, C.L. Beyler, W. Douglas Walton, R.L.P. Custer, J.R. Hall Jr, and J.M. Watts Jr, *SFPE handbook of fire protection engineering*, 3rd ed. (Quincy, Massachusetts, National Fire Protection Association, 2002), pp. A30-A33.

[18] E.C. Robertson, *Thermal properties of rocks*, United States Geological Survey (Open-File Report, 88–441), 1988), pp. 47.

[19] D.W. Waples and J.S. Waples, *Nat. Resour. Res.* 13, 97 (2004).

[20] J.A. Diaz, Z. Ye, X. Wu, A.L. Moore, R.J. Moon, A. Martini, D.J. Boday, and J.P. Youngblood, *Biomacromolecules* 15, 4096 (2014).

[21] Y.I. Cho, H.K. No, and S.P. Meyers, *J. Agric. Food Chem.* 46, 3839 (1998).

[22] T. Hatakeyama, K. Nakamura, and H. Hatakeyama, *Polymer* 23, 1801 (1982).

[23] R.C. Progelhof, J.L. Throne, and R.R. Ruetsch, *Polym. Eng. Sci.* 16, 615 (1976).

[24] J. Wang, J.K. Carson, M.F. North, and D.J. Cleland, *Int. J. Heat Mass Transfer* 49, 3075 (2006).

[25] N. Simpson, R. Wrobel, and P.H. Mellor, *IEEE Trans. Ind. Appl.* 49, 2505 (2013).